ICAM International Conference on Agile Manufacturing

Structural Design of Nanopositioners Fabricated from Different Metal Alloys in Terms of Their Stiffness, Stresses, and Modal Frequency.

Nathanael A. Miller, A.A. Elmustafa[¥]

Department of Mechanical Engineering, Old Dominion University

Norfolk, VA 23529 USA

Abstract: In this paper, we discuss the calculations of stiffness, stresses, and modal frequency of a single-axis, piezo-driven horizontal guided motion nanopositioning stage. This stage is designed for precision machining processes, such as magnetic storage, medical equipment, and space deployable structures. Piezoelectric actuators with their smooth motion, infinite resolution, and high stiffness are commonly coupled through flexure-hinged mechanical displacement amplifiers. This paper discusses aspects of the design parameters such as stiffness, stresses, and modal frequency of the flexure hinges for such structures. These parameters are calculated using both the finite element method (FEM) and theoretical analysis. The theoretical model and the equations involved in the derivation of the deflected shape of the flexural hinges were presented elsewhere. As well, in this study, we will present a comparison between nanopositoners fabricated from aluminum 7075, stainless steel 304, and invar 36 alloys in terms of their flexural hinge stiffness, stresses, and modal frequencies. The stresses of the flexural hinges were monitored not to exceed the yield point of the base metal.

Keywords: flexural hinge, nanopositioner, precision machining, piezoelectric actuator, finite element simulations, invar alloy, aluminum alloy.

1. Introduction

Optical, medical, space-deployable, and many other devices continue to advance rapidly and resourcefully at the same time they continue to decrease in size and shape. There is an increasing demand for a smaller, faster, more densely packed and controlled structures (smoother and more accurate in shape). Electronics, optics, micro-electro-mechanical-systems (MEMS), magnetic storage, medical equipment, and space-deployable structures are examples of mechanical devices that incorporate electrical or magnetic features. Many of these devices rely on precision motion [1-11]. In precise guided-motion processes there is a need for low-profile, high-stiffness, and large-load carrying ability nanopositioning stages.

Piezoelectric actuators (PZTs) with their smooth motion, near-infinite resolution, and high stiffness became an attractive alternative to replace electrical and mechanical devices used in precise guided-motion stages.

Piezoelectric materials experience dimensional changes when they are subject to an electric field [2]. This feature possesses a broad value. The dimensions of a piezoelectric material can be controlled to a resolution of the order of a thousandth of a nanometer or less depending on thermal noise and the noise of the driving voltage. Moreover, piezoelectric devices are driven over millions of cycles without wear or deterioration, their response time is in microseconds, and the momentous property they possess is that they can move large masses. Therefore, they are well-suited for sensor, actuator, and positioner applications.

In this study, we compare single-axis, piezo-driven, horizontally-guided motion nanopositioners fabricated from aluminum 7075, stainless steel 304, and invar 36 alloys in terms of their flexural hinge stiffness, stresses, and modal frequencies. The stresses of the flexural hinges were monitored to ensure that the allowable stresses of the base metal were not exceeded.

[¥] Corresponding author

2. Nanopositioner Structure

The nanopositioner stage of Figure 1 is 100 *mm* by 100 *mm* and 18 *mm* thick. The nanopositioner has two parts: a mechanical structure machined from a single metal and a piezoelectric actuator that is mounted in a cavity at the back of the mechanical structure. The mechanical structure is composed of the structure body, where a probe or device resides, and four flexural hinges. The nanopositioner stage is bolted to a footprint that cannot allow motion in any directions [5]. Each flexural hinge dimension is 16 *mm* by 18 *mm* and 1.0 *mm* thick as indicated by Figure 1.b

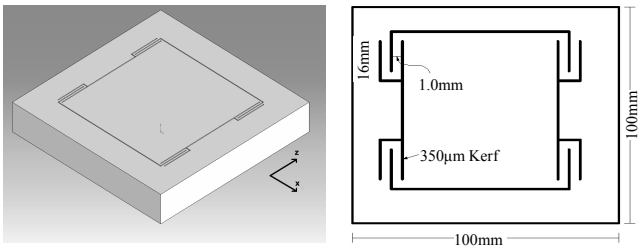

Figure 1. A flexural-hinge guided-motion. The outer frame is secured to a footprint and a probe or a device is secured to the inner stage. The PZT actuator is housed in a cavity in the bottom of the stage. (not shown)

Using electric discharge machining (EDM), in this case a kerf width of 350 μm is used, the flexural hinges are machined and shown as part of the positioner stage of Figure 1.a.

The flexural hinges provide the guided motion of the stage via the horizontal motion of the piezoelectric actuator positioned inside the structure of the stage. When a voltage is applied to the piezoelectric actuator, the actuator expands and generates a driving force that causes the flexural hinges to deflect and achieve the precise motion in the horizontal direction.

	Young's modulus Gpa	Pisson's ratio	Yield tensile strength Mpa	Density g.cm3	Coefficient of Thermal Expansion (20ºC, µm/m-ºC)
Al 7075	72	0.33	435	2.81	23.60
SS 304	200	0.31	690	7.90	16.60
Inv 36	148	0.30	483	8.05	1.30

Table 1. Physical and mechanical properties of aluminum (Al) 7075, stainless steel (SS) 304, and carpenter invar (Inv) 36.

Three different materials are used for simulation: aluminum 7075, stainless steel 304, and carpenter invar 36 alloys. The physical and mechanical properties of these alloys are indicated in Table 1.

The four flexural hinges are represented by four sets of springs; two springs per hinge. Each set is composed of two top and bottom springs of stiffness K_T and K_B connected in parallel. In designing the stage, the equations of the deflected shape of the top and bottom hinges derived in [6] are used to calculate the stiffness, stresses, and modal frequencies in the flexural hinges. The stiffness of the top part of the flexural hinge is given by [6]

$$K_T = \frac{12EI}{L^3}, \tag{1}$$

E is the modulus of elasticity of the material, I is the moment of inertia of the flexural hinge, and L is the effective length of the flexural hinge. The stiffness of the bottom part of the flexural hinge is given by

$$K_B = \frac{6EI}{L^3}. \tag{2}$$

Therefore, we can derive $K_1 = K_2$ as [12]

$$K_1 = K_T + K_B, \tag{3}$$

and similarly, $K_3 = K_4$.

The stiffness $K_{13} = K_{24}$ is given by [12]

$$K_{13} = \frac{1}{\frac{1}{K_1}} + \frac{1}{\frac{1}{K_3}}, \tag{4.a}$$

and

$$K_{24} = \frac{1}{\frac{1}{K_2}} + \frac{1}{\frac{1}{K_4}} \tag{4.b}$$

Therefore, the effective stiffness, K_{eff} is given by

$$K_{eff} = K_{13} + K_{24}. \tag{5}$$

Using equation 1 through 5, we can obtain the effective stiffness as follows

$$K_{eff} = \frac{18EI}{L^3}. \tag{6}$$

In the following sections, static as well as dynamic analysis is performed to study the stresses and modal frequencies of the nanopositioners.

3. Dynamic analysis

The flexural-hinge nanopositoner stage of Figure 1 can be dynamically modeled as a collection of four sets of springs and the main body of the stage mass. It is assumed that the flexural-hinge nanopositoner structure has a constant stiffness and mass effects, no damping effects, and the structure has no time varying forces, displacements, pressures, or temperature applied (free vibration).

3.1 Description of analysis

The equation of motion expressed in matrix notation using the above assumptions can be written as [12]

$$[M]\left\{\ddot{U}\right\} + [K]\{U\} = \{0\}. \quad (7)$$

For a linear system, free vibrations will be harmonic of the form:

$$\{U\} = \{\phi_i\}\cos\omega_i t, \quad (8)$$

where $\{\phi_i\}$ is the eigenvector representing the mode shape of the i^{th} natural frequency. ω_i is the natural circular frequency in radians per unit of time, and t is the time.

Therefore differentiating equation 8 twice, and after substitution, equation 7 can be written as:

$$(-\omega_i^2[M] + [K])\{\phi_i\} = \{0\}, \quad (9)$$

equation 9 is satisfied if either $\{\phi_i\} = \{0\}$ or if the determinant of $[K] - \omega^2[M]) = \{0\}$. The first option is the trivial solution, which is not of interest. Thus, the second option gives the solution

$$[K] - \omega^2[M]) = \{0\}. \quad (10)$$

This is an eigenvalue problem, which can be solved for up to n values of ω^2 and n eigenvectors $\{\phi\}_i$, which satisfy equation 9. n is the number of mode shapes desired. The natural frequency f is commonly used instead of the circular natural frequency, ω. The relationship between the natural frequency f and the circular natural frequency ω is given by

$$f = \frac{1}{2\pi}\omega. \quad (11)$$

4. Static analysis

The flexure formula is given by [13]

$$\sigma = \frac{M x}{I}, \quad (12)$$

where σ is the normal stress at the intermediate distance x, M is the resultant internal moment computed about the neutral axis of the cross section, I is the moment of inertia of the cross-sectional area computed about the neutral axis, and x is the perpendicular distance from the neutral axis to the point where the stress is sought. It is assumed that the member is straight, has a symmetric cross section, and is made of homogeneous linear-elastic material so that Hooke's law applies. The flexural hinges of the guided-motion nanopositioner stage are modeled as prismatic flexural beams. Since the loadings are applied perpendicular to flexural hinges' longitudinal axis, the flexure formula can be used to calculate the stiffness and stresses in the flexural hinges.

The maximum internal bending moment of the flexural hinge occurs at the fixed support and is given by [6]

$$M = \frac{PL}{2}, \quad (13)$$

where P is the force applied perpendicular to the longitudinal axis of the hinges. Substituting equations 1 and 13 into equation 12, the maximum deflection, δ_{max}, is given by [14]

$$\delta_{\max} = \frac{\sigma_{\max} L^2}{3Ed}, \quad (14)$$

where $d = 2x$, and σ_{max} is the maximum stress at the section of maximum bending moment.

5. Finite element modeling

A finite element model of the stage with four flexural hinges is built using the multipurpose finite element code ANSYS version 5.5.1 [15]. The nanopositioner stage and the flexural hinges are modeled using 8-nodes SOLID45 structural elements. The study combined linear elastic static and dynamic analysis. Boundary conditions are applied through the corners of the stage to hold the positioner frame in place. Rotations as well as translations are constrained at these corners in the three directions. A transverse load, generated by the piezoelectric actuator positioned inside the cavity at the back of the nanopositioner, is applied at four key points. A 25 μm displacement is used instead of applying a force, and the applied force is deduced from the results.

6. Theoretical and FEM Simulation Results

As mentioned in the introduction, the stiffness, stresses, and modal frequencies of the guided-motion flexural-hinge nanopositioners are calculated using the FEM and compared with the analytical solution obtained here and in [6]. Flexural-hinge guided-motion nanopositioers driven by piezoelectric actuators and driver electronics resonates at a few hundred cycles per second (Hz) when no additional mass is added to the stage. Eventually a mass has to be added to the stage and that causes the resonant frequency of the stage to decrease depending on the device or probe that the stage has to move. Piezoelectric actuators' resonant frequency is estimated in thousands of Hertz (typically, 7-10 kHz) depending on the actuator model, shape, and size. The driver electronics resonates at few hundred thousands Hertz (typically, 100-150 kHz).

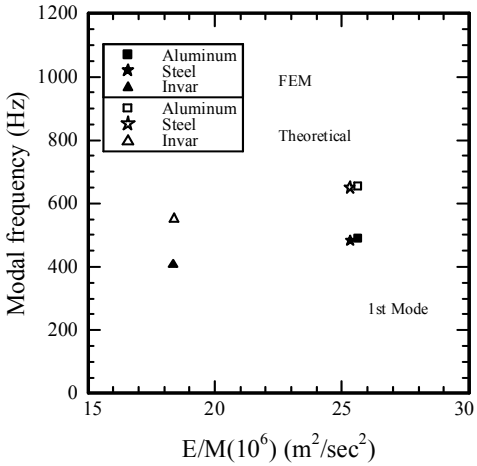

Figure 2. 1st modal frequency for the three alloys, aluminum, stainless steel, and invar.

It is therefore the nanopositioner resonant frequency that is critical for a single loop to control. Figure 2 shows the first modal frequency from a FEM solution compared with the first modal frequency using equations 6 and 11. The modal frequencies are plotted versus the normalized elastic modulus and mass.

The stresses calculated using the FEM are compared with the theoretical calculations using equation 14 as shown in Figure 3. Traditionally, when designing a structure, the design criteria are based on the fact that stresses should not exceed the allowable stress limit. The design and construction of the nanopostioner stage addressed in this paper followed such a criteria and the stresses were monitored not to exceed the allowable stress limit. The allowable stress limit for the metal springs is based on 10% of the allowable stress limit for the base metal as described by [14].

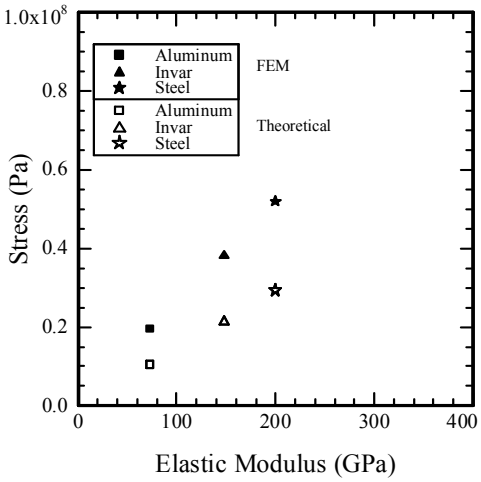

Figure 3. FEM and theoretical stresses for the three alloys.

The forces in the nanopositioners calculated using the FEM are compared with the forces calculated using the effective stiffness derived in equation 6 and a prescribed displacement of 25 μm as shown in Figures 4 in 3D from a FEM simulation for stainless steel 304.

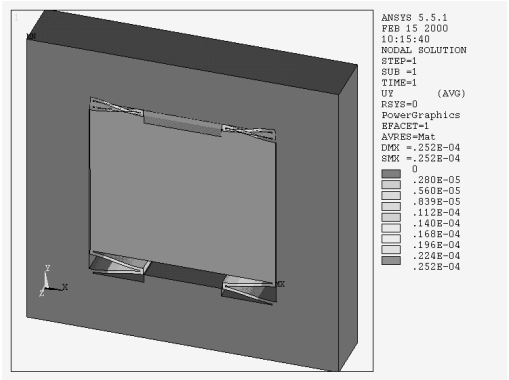

Figure 4. 3D eight-node structural solid element mesh of the four flexural hinges of the guided-motion nanopositioner stage of Figure 1. BC's are prescribed on the four corners.

7. Increasing Performance

To avoid penalties such as cost and high voltage needs associated with piezoelectric actuators that have large displacement, it is desirable to reduce the necessary travel of the actuator. To do this, a feature designed to amplify the output of the PZT is added. This feature, called the lever arm, seen in Figure 5, is a cantilever beam supported with a single flexure hinge element at each end. As seen in Figure 5.b, the PZT acts at one end of the beam causing the other end to push the translation stage.

The most interesting result is the overall travel of the stage in comparison to the input displacement. As with the ANSYS analysis, it is also critical that the structure does not experience plastic deformation. Finally, it is

important that out-of-plane displacement is kept to a minimum.

To evaluate performance of the lever arm, the design is modeled using SolidWorks 2005 and analyzed using the multipurpose finite element code ABQUAS v6.5. A static analysis is performed on the structure, given a transverse load applied at the base of the arm. This simulates the effect of the PZT, and displaces the lever arm to set 35μm. The same boundary conditions used in ANSYS apply in this analysis.

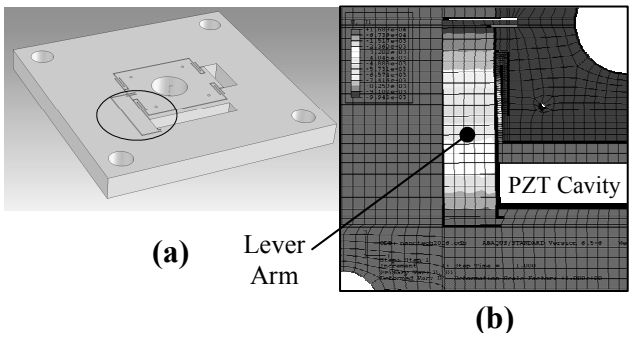

Figure 5. The positioner structure with the lever arm a) as modeled in SolidWorks, and b) as analyzed in ABAQUS

The addition of the lever arm to the design causes a 100μm displacement of the inner stage, which is about three times the displacement of the PZT. This is accomplished with negligible undesired out-of-plane displacement. Future work will include dynamic analysis of the entire positioner structure with the lever arm, and will also take into consideration the adverse dynamic effects of ceramic PZT.

8. Discussion

As stated in the introduction, an objective of this work is to determine and compare stiffness, stresses, and modal frequencies from a FEM simulation with an analytical solution for three different alloys, aluminum 7075, stainless steel 304, and invar 36. From Figure 2, we can infer that the resonant frequency predicted by the FEM simulation and the theoretical solution differ by as much as 25% for the three different alloys, yet, the resonant frequency predicted by the FEM simulation is lower than the frequency estimated by the theoretical solution. If a design criteria is based on selecting an alloy that possess a higher resonant frequency, certainly, one would choose either the aluminum or stainless steel alloys, but the invar alloy would be a better choice if the coefficient of thermal expansion is considered as a criteria as well. (CTE for invar is 1.3 as compared to 23.6 and 16.6 for aluminum and stainless steel, respectively as indicated in Table 1). It was concluded in [2] in a study for out-of-plane displacement due to a transverse load applied to the nanopositioner, in a comparison between aluminum 7075 and invar 36, that the out-of-plane displacement in the invar 36 is about half of that in the aluminum 7075. The invar 36 is considered UHV (ultra-high-vacuum) compatible as compared to the other alloys. Another factor of equal importance is that wire EDM, an invar alloy, is not as fundamental as in the case of aluminum and stainless steel, moreover wire EDM, an invar nanopositioner, is done by few machine shops and costs more.

Another objective is to calculate the stresses and forces in the nanopositioners, and correlate the results with the FEM simulations. It is verified that the allowable stress limit is not exceeded. Although the stresses predicted by the FEM simulation in Figure 3 are higher than those predicted by the exact solution, the allowable stress limit is not exceeded. The allowable stress limit is established based on 10% of the base material as suggested by [14]. From Figure 6, it is observed that the FEM and the exact solution diverge as the elastic modulus increases, and they converge as the modulus decreases.

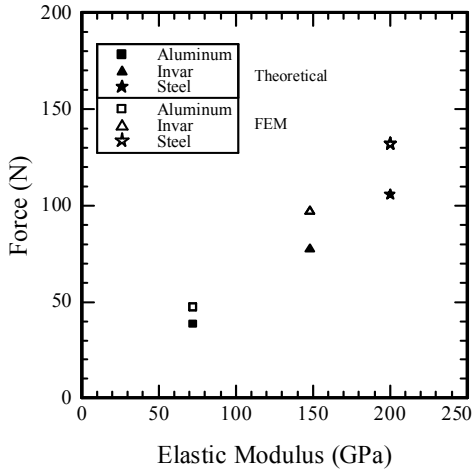

Figure 6. FEM and theoretical transverse forces for the three alloys. A 25 μm range of motion is used for these simulations

It is tangible that aluminum is the best choice among the three alloys in terms of the proximity of the theoretical solution to the FEM simulation, whereas stainless steel is the least likeable choice in this case, however, the results reached by the FEM simulations for the three alloys are still reliable. The correlation of the FEM simulation with the theoretical calculations for the transverse forces in the nanopositioners is shown in Figure 6. The results of the comparison indicate that the magnitude of the forces of the FEM simulations agree to within 18% of the theoretical calculations. Based on the comparison of Figure 6, there is confidence on the reliability of the FEM simulations.

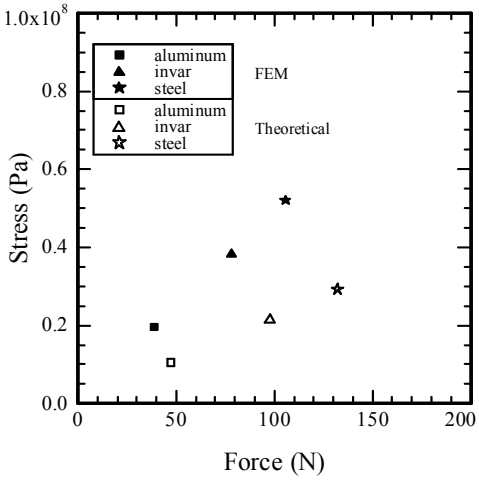

Figure 7. Stresses versus transverse forces in the hinges. A 25 μm range of motion is used for these simulations.

We can take the data in Figures 3 and 6, which represent the FEM simulation and the theoretical calculations for the forces and stresses in the three alloys and combine them in Figure 7. The stresses are plotted versus the applied nanopositioner force. With the aid of Figure 7, an alloy can be appropriately selected for a specific piezoelectric actuator driving force. The allowable stresses in the flexural hinges can be verified using Figure 6.

9. Summary and Conclusion

The guided-motion nanopositioner assembly consists of four sets of flexural hinges and the body of the nanopositioner stage. Each flexural hinge contains a top and bottom prismatic beam with stiffness K_T and K_B respectively. The results represent a comparison between three different alloys, aluminum 7075, stainless steel 304, and invar 36 in terms of their stiffness, stresses, and modal frequencies. A detailed discussion on the criteria of appropriately selecting a particular alloy as a potential candidate for a nanopositioner stage construction is presented. Among the various design parameters included in the discussion (stresses, stiffness, and natural frequency of vibration), a comparison based on the coefficient of thermal expansion (CTE), ultra-high-vacuum (UHV) compatibility, wire electric discharge machining (WEDM), and cost of production is presented as well.

In summary, a detailed FE analysis, as well as theoretical calculations of a flexural-hinge profile, piezo-driven, horizontal guided-motion nanopositioner stage that is intended for use in precision machining applications is presented. This paper describes the theoretical calculations and FEM simulations of stiffness, stresses, and modal frequency of a single-axis, piezo-driven, horizontal guided-motion nanopositioning stage. The analytical solution is compared with the FEM simulations. It is concluded that the two solutions compare well.

10 References

1. Yang R, Jouaneh M, Schweizer R. Design and characterization of a low-profile micropositioning stage. Precision Engng 1996; 18: 20-29.
2. Xu WL, Han L. Piezoelectric actuator based active error compensation of precision machining. Meas. Sci. Technol 1999; 10: 106-111.
3. Xu W, King T. Flexure hinges for piezoactuator displacement amplifiers: flexibility, accuracy, and stress consideration. Precision Engng 1996; 19: 4-10.
4. Awabdy BA, Shih WC, Auslander DM. Nanometer positioning of a linear stage under static loads. IEEE Trans. Mechatronics 1998; 3(2): 113-119.
5. Elmustafa AA, Lagally MG. Flexural-hinge guided motion nanopositioner stage for precision machining: finite element simulations. Precision Engng 2000; 25(1): 77-81.
6. Elmustafa AA. Theoretical and Finite Element Approach: Flexural Hinge Guided Motion Nanopositoners for Precision Machining (submitted).
7. Yang R, Jouaneh M. Design and analysis of a low profile micro-positioning stage. Technology and Machine Development and Improvement, ASME 1992; 58: 131-142.
8. Kim JD, Kim DS. Waviness compensation of precision machining by piezo-electric micro cutting device. Int J Mach Tools Manufact 1998; 38: 1305-1322.
9. Meli F, Thalmann R. Long-range AFM profiler used for accurate pitch measurements. Meas. Sci. Technol 1998; 9: 1087-1092.
10. Homann BS, Thornton AC. Precision machine design assistant: A constraint-based tool for the design and evaluation of precision machine tool concepts. AI EDAM 1998; 12: 419-429.
11. Arcona C, Dow TH. An Empirical Tool Force Model for Precision Machining. Transactions of the ASME 1998; 120: 700-707.
12. William TT, Marie DD. Theory of Vibration with Applications, Prentice Hall, 1998.
13. Beer FP, Johnston ER. Mechanics of Materials, McGraw-Hill, Inc, 1998.
14. Smith ST, Chetwynd DG. Foundations Of Ultraprecision Mechanism Design Gordon and Beach Science Publishers, 1992.
15. ANSYS finite element program 1999.